Kinetic Resolution of Peptide Bond and Side Chain Far-UV Circular Dichroism during the Folding of Hen Egg White Lysozyme†

Alain F. Chaffotte, Yvonne Guillou, and Michel E. Goldberg*

Unité de Biochimie Cellulaire, CNRS URA 1129, Institut Pasteur, 28 rue du Dr. Roux, 75724 Paris Cedex 15, France

Received April 21, 1992; Revised Manuscript Received July 16, 1992

ABSTRACT: The kinetics of regain of the native ellipticity in the far- and near-UV spectra have been investigated during the refolding at pH 7.8 and 20 °C of guanidine-unfolded, nonreduced hen egg white lysozyme. Stopped-flow studies showed that the ellipticities at 260 and 289.5 nm exhibit biphasic kinetics with rate constants of about 50 s^{-1} and 2.5 s^{-1} for the rapid and slow phase, respectively. The ellipticity in the far-UV obeyed triphasic kinetics. In addition to a rapid and a slow phase with rate constants similar to those observed in the near-UV, a "burst" of ellipticity was shown to occur in the dead time of the experiments. The effects of low pH and of concentrations of guanidine ranging from 0.075 to 1.5 M on the rapid and slow rate constants were studied. Under all conditions investigated, the rate constants observed in the far- and near-UV for a given phase were the same, thus suggesting that the molecular events observed in the two regions of the UV spectrum are either identical or strongly coupled. Continuous-flow experiments at different wavelengths between 214 and 240 nm under conditions where the dead time for the observation was only 4 ms, followed by a detailed analysis of the kinetics of ellipticity change at each wavelength, provided the spectrum of the molecular species formed at the end of the burst phase. This spectrum was found to closely fit that predicted from the secondary structure of native lysozyme. It was shown that the changes in far-UV ellipticity that occur during the rapid and slow phases do not reflect significant changes in the secondary structure of the polypeptide chain. Rather, they reflect essentially changes in the state of side chains, with an important contribution arising from disulfide bonds. Thus, the complete nativelike secondary structure of lysozyme seems to be practically formed in less than 4 ms.

Recent advances in studies on the mechanisms of protein folding have shown the existence of well-defined intermediates which seem to be a crucial part of the folding mechanism (Kim & Baldwin, 1982, 1990; Creighton, 1990; Baldwin, 1991; Baldwin & Roder, 1991). This is especially true for very early folding intermediates, since it is now well established that the determining steps that orient the polypeptide chain toward its native conformation occur very early in the folding process. Indeed, several essential features of the native protein, i.e., elements of nativelike secondary and tertiary structure, are already persent very early in the game (Udgaonkar & Baldwin, 1988; Roder et al., 1988; Bycroft et al., 1990; Briggs & Roder, 1992). Yet, a key question that remains unanswered concerns the mechanisms leading to these early intermediates. Two extreme models deal with this question. The "framework" model (Kim & Baldwin, 1982) postulates that the initial event is the formation of nativelike secondary structure elements, stabilized essentially by local interactions, which constitute the framework for the tertiary structure of the polypeptide chain. On the contrary, Dill (1985) postulates an initial hydrophobic condensation of the polypeptide chain driven essentially by nonspecific long-range hydrophobic interactions. In between these two extremes, the "subdomain" model of Oas and Kim (1988) postulates a tight coupling between specific local and long-range interactions. A better understanding of these early folding steps will obviously require a precise structural and kinetic characterization of the earliest detectable folding intermediates experimentally accessible.

Folding intermediates have been characterized so far by observing folding kinetics with different conformational probes. Thus, early events dealing with the formation of the protein secondary structure could be monitored either by far-UV circular dichroism to estimate the total content in secondary structure (Kuwajima et al., 1985, 1991; Labhardt, 1986; Pflumm et al., 1986) or by pulsed amide proton exchange to monitor the presence of stable hydrogen-bonded structures (Udgaonkar & Baldwin, 1988; Roder et al., 1988; Bycroft et al., 1990; Briggs, & Roder, 1992). The pulsed amide proton exchange followed by NMR[1] analysis of the protected protons provides a precise description of the kinetics of formation of individual hydrogen bonds. But it can detect only hydrogen bonds that belong to stable intermediates and that are strongly protected from exchange in the native state. Consequently, nonnative structural elements, or elements not yet stable enough under the labeling conditions, will escape observation by the pulsed amide proton exchange method. On the contrary, the peptide far-UV circular dichroism provides a measure of the total content in α-helices and β-structures. Though it gives no information on their position within the polypeptide chain, it can detect the presence of secondary structure elements even if they are not stable or nonnative. However, the far-UV CD spectrum of a protein may not reflect only its secondary structure because of possible contributions to the far-UV ellipticity of side chains from aromatic or cystinyl residues (Sears & Beychok, 1979; Manning & Woody, 1989). This often renders problematic the decomposition of equilibrium CD spectra in terms of α-helices and β-structures. We thought that, in some cases, this difficulty might not impair the study of early folding intermediates. Indeed, several reports indicate that early folding intermediates present after 15–20 ms of folding exhibit a large far-UV CD signal but no near-UV CD [see review by Kuwajima (1989)]. The absence

† This research was supported by funds from the Institut Pasteur, the Université Paris 7, and the Centre National de la Recherche Scientifique (URA 1129).

[1] Abbreviations: BPTI, bovine pancreatic trypsin inhibitor; CD, circular dichroism; GuHCl, guanidine hydrochloride; HEL, hen egg white lysozyme; NMR, nuclear magnetic resonance.

0006-2960/92/0431-9694$03.00/0

of ellipticity in the near-UV indicates that in these intermediates the cystinyl and aromatic residues are in an isotropic environment and hence should not contribute to the far-UV CD spectrum. This prompted us to investigate such early folding intermediates, taking advantage of the recent developments in the CD stopped-flow technology that now permit one to monitor the kinetics of ellipticity changes with a dead time of only 4 ms.

Hen egg white lysozyme was chosen as a model protein for this study because it is one of the best characterized proteins in terms of conformation. Its 3D structure has been solved to high resolution by X-ray crystallography (Blake et al., 1965). Complete proton NMR assignments have been reported (Redfield & Dobson, 1988) and it is likely that the folding kinetics will soon be investigated in detail by pulsed amide proton exchange. Its folding properties, both at equilibrium and in kinetics, have been extensively investigated (Tanford et al., 1966; Aune & Tanford, 1969; Tanford, 1970; Kato et al., 1981; Dobson & Evans, 1984). In particular, it is well known that the protein refolds efficiently and rapidly under a variety of environmental conditions if its disulfide bonds have not been reduced in the unfolded state. Moreover, the native protein exhibits large CD signals, both in the near-UV because it contains a large number of aromatic residues and in the far-UV since it contains a high proportion of α-helices (Blake et al., 1965). Furthermore, circular dichroism kinetic studies have already been performed (Kuwajima et al., 1985; Ikeguchi et al., 1986). They showed that over 80% of the native CD signal at 222.5 nm was already regained at a stage of the folding where the near-UV ellipticity remained essentially zero, thus suggesting that the analysis of the transient intermediate CD spectrum in terms of secondary structure ought to be reliable. We therefore chose to reinvestigate, in more detail and with a better time resolution, the regain of the near- and far-UV signals during the renaturation of HEL with intact disulfides.

MATERIALS AND METHODS

Enzyme and Chemicals. Hen egg white lysozyme was obtained from Boehringer-Mannheim. Guanidine hydrochloride (ultra pure) was from Schwarz-Mann-ICN. All other chemicals were reagent grade.

Buffer A was 0.07 M NaCl adjusted to pH 1.6 with concentrated HCl, and buffer N was 0.01 M potassium phosphate, pH 7.8.

Sample Preparation. Lysozyme was dissolved in buffer N (for native lysozyme) or in buffer N containing 6 M GuHCl (for denatured lysozyme). The protein concentration was determined spectrophotometrically, using a specific extinction coefficient of 2.5 mg^{-1} cm^2. The protein concentration was then adjusted to 8 mg/mL for far-UV or 25 mg/mL for near-UV studies, by addition of the appropriate volume of the same buffer or GuHCl solution. The solutions of denatured protein were incubated at 4 °C for at least 1 h and no more than a day.

Renaturation Buffer. The renaturation buffer was either buffer A or buffer N, depending on the pH chosen for the refolding experiment.

Equilibrium and kinetic circular dichroism measurements were performed in a CD6 spectrodichrograph (Jobin-Yvon/Instruments S.A., Longjumeau, France) equipped with the stopped-flow optional accessory. This accessory is based on a SFM3 stopped-flow module (Bio-Logic, Claix, France) which is coupled to the CD6 by means of the mechanical, optical, electronic, and software kit provided by Jobin-Yvon. The observation cell used was a 5-mm optical path T50/15 transmission cell. The stopped-flow module (reservoirs, syringes, mixers, and observation cell) were thermostated at 20 ± 0.1 °C by means of a temperature-controlled water bath and a high-flow TE4 MO-HC circulation pump (Little Giant Pump Co., Oklahoma City, OK). Two 18-mL and one 5 mL syringe were used, the two large ones injecting into the first mixer and the small one into the second mixer.

Equilibrium spectra were obtained by recording, in scanning mode, the CD spectrum of denatured (in 6 M GuHCl) or refolded lysozyme solutions (0.1 mg/mL) directly in the stopped-flow observation cell and subtracting the spectrum of the corresponding solvent. The integration time was 2 s, and the wavelength interval was 1 nm. The spectra shown are the results of averaging at least three accumulations.

For the kinetic studies, the volumes injected and the duration of the injections will be described for each experiment. They resulted in a dead time of 4 ms. For the refolding experiments, the denatured protein in 6 M GuHCl contained in the small syringe was diluted 80-fold with renaturation buffer contained in the two large syringes. Data were collected with sampling intervals and filtering constants ranging from 1 to 20 ms, as indicated for each experiment.

The kinetics were analyzed as follows. Each experiment was repeated 30–120 times (as indicated) and the accumulated kinetic data were averaged. The averaged data file was converted into as ASCII file by the ISA/hda ASCII conversion subroutine of the CD6 software. The resulting file was, when needed, reduced to 1000 data points, and deconvolution into exponentials was achieved by means of the Fig.P 5.0 program (Biosoft, Cambridge, U.K.).

RESULTS

Renaturation at Neutral pH. HEL, denatured with 6 M GuHCl in buffer N, was diluted 80-fold in buffer N and the CD was monitored at 222 nm to follow the kinetics of formation of secondary structure. The results of a typical experiment are shown in Figure 1A. As expected from the spectra of unfolded and native lysozyme (see Figure 5), the refolding was reflected by an overall decrease of the ellipticity. However, the kinetics of the CD change were complex. Thus, the ellipticity first decreased in a time range just above the dead time of the stopped-flow instrument. It then slowly increased to finally reach the value of the native enzyme. The observed kinetics could be satisfactorily fitted to a double-exponential process in which the fast phase (ellipticity decrease) had a rate constant of 62 ± 11 s^{-1} and the slow phase (ellipticity increase) had a rate constant of 2.3 ± 0.1 s^{-1}. Moreover, the extrapolation of the fast phase to time zero of the recording (i.e., 6 ms after the mixing) yielded a value of −23.9 mdeg for the ellipticity. Under these experimental conditions, the ellipticity determined for the denatured protein in buffer N was only −15.5 mdeg. This indicated that the rapid phase characterized above was in fact preceded by an even faster one that was completed during the dead time of the stopped-flow instrument. Thus, the far-UV CD signal obeyed complex kinetics that could be decomposed in at least three very distinct phases (see Table I).

It has been reported that the side chains of aromatic residues can contribute significantly to the protein ellipticity at wavelengths around 220 nm. The tight packing of aromatic side chains might therefore be responsible for some of the ellipticity changes at 222 nm observed during the refolding of HEL. To test this possibility, the kinetics of regain of the near-UV CD were studied at wavelengths characteristic of the tryptophans and of the tyrosines and phenylalanines. The ellipticity change at 289.5 nm, which mainly reflects the change in the environment of tryptophan residues, was observed first. It appeared to obey biphasic kinetics (Figure 1B). The rate

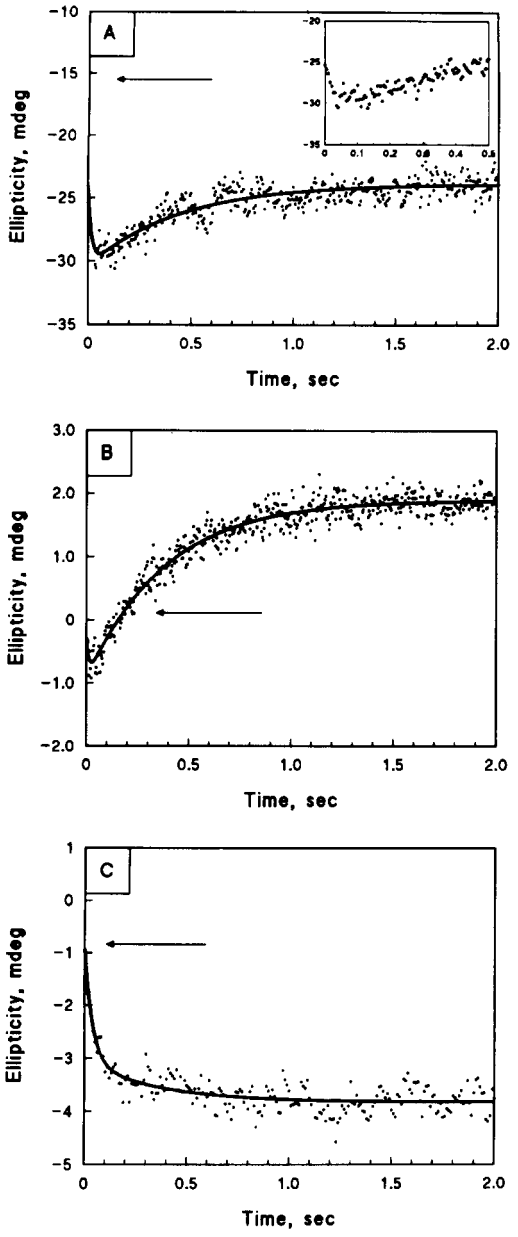

FIGURE 1: Kinetics of ellipticity changes upon folding of HEL at pH 7.8. HEL in 6 M GuHCl at pH 7.8 (from the small syringe) was mixed with buffer N (from the large syringes). The duration of the injection was 140 ms, resulting in a 6-ms dead time. Recording of the ellipticity was triggered at the end of the injection. The horizontal arrow indicates the value of the ellipticity of unfolded HEL in buffer N, obtained by sequential injections of 6 M GuHCl, HEL in 6 M GuHCl, buffer N, and HEL in buffer N as described by Chaffotte et al. (1991). The solid line represents the best fit of bi- or triphasic (as indicated below) sequential kinetics to the experimental points. (A) Ellipticity at 222 nm: 10 μL of denatured HEL (8 mg/mL) and 790 μL of buffer N were injected. The resulting concentration of HEL in the observation cell was 0.1 mg/mL. The sampling interval and filtering constant were 5 ms. The number of kinetics accumulated was 126. The fit shown was with triphasic kinetics. Inset: enlarged view of the first 500 ms of the kinetics. (B) Ellipticity at 289.5 nm and (C) ellipticity at 260 nm: 15 μL of denatured HEL (25 mg/mL) and 735 μL of buffer N were injected. The resulting concentration of HEL in the observation cell was 0.5 mg/mL. The number of kinetics accumulated was 120, the sampling interval was 4 ms, and the filtering constant was 2 ms at 289.5 nm. The number of kinetics accumulated was 90, and the sampling interval and filtering constant were 10 ms at 260 nm. The fit was for biphasic kinetics.

constants of the two phases, determined by fitting the data to a two-exponential process, were 2.6 ± 0.1 s^{-1} for the slow phase and 80 ± 30 s^{-1} for the rapid phase. These values are close to those obtained for the slow and rapid phases at 222 nm (see above). Moreover, the sum of the amplitudes of the two phases (1.8 ± 0.2 mdeg) was close to the total ellipticity change at 289.5 nm (1.6 ± 0.2 mdeg), indicating that no significant very rapid ellipticity change could be detected at this wavelength during the dead time of the stopped flow. The ellipticity change at 260 nm, which reflects predominantly the tight packing of tyrosine and phenylalanine side chains, also obeyed biphasic kinetics (Figure 1C). The fast phase (amplitude of –2.2 mdeg) had a rate constant of 26 ± 6 s^{-1} and the slow phase (amplitude of –0.7 mdeg) had a rate constant of 2.8 ± 0.6 s^{-1}. The difference between the ellipticities of native and unfolded HEL under these experimental conditions (–3 mdeg) was, within experimental error, equal to the sum of the amplitudes of the two phases. Thus, in addition to the very rapid phase of CD change at 222 nm that was not accompanied by changes in the near-UV ellipticity, two phases have been identified that gave rise to changes in ellipticity of different signs and amplitudes depending on the wavelength. One had a rate constant in the range of 30–80 s^{-1} and the other had a rate constant of 2.3–2.8 s^{-1}.

Table I: Rate Constants and Amplitudes of the Kinetic Phases Observed by CD during the Folding of HEL at pH 7.8[a]

wavelength (nm)	phase	rate constant (s^{-1})	amplitude[b] (%)
222	burst	>250	101
	rapid	62 ± 11	75
	slow	2.3 ± 0.1	–75
260	burst		0
	rapid	26 ± 6	76
	slow	2.8 ± 0.6	24
289.5	burst		0
	rapid	80 ± 30	–54
	slow	2.6 ± 0.1	154

[a] The kinetic parameters at each wavelength are those obtained for the best fit of the experimental data of Figure 1 to a biphasic (at 260 and 289.5 nm) or triphasic (at 222 nm) process. [b] The amplitudes are expressed as a percentage of the difference between the ellipticities of native and denatured HEL.

In order to check that these two phases of ellipticity change did not correspond to artifacts due to transient birefringence, cavitation, or cell deformation caused by the flow during or just after the mixing, the following control experiment was carried out. Since HEL is known to be quite stable in urea at neutral pH, HEL was dissolved and dialyzed against buffer N containing 8 M urea. The CD spectrum was recorded and compared to that of HEL without urea. As expected, 8 M urea in buffer N and at 20 °C was ineffective in modifying the CD spectrum of HEL (data not shown). A 10-μL aliquot of HEL in 8 M urea was then injected with 790 μL of buffer N over 140 ms, and the ellipticity at 222 nm was monitored. No variation in the CD signal was detected throughout the time range investigated (from 6 ms up to 15 s after the mixing), at all the sampling times used, i.e., down to 1 data point/ms (data not shown). This demonstrated that the ellipticity changes observed during the refolding of GuHCl-unfolded HEL indeed reflected folding steps and not experimental artifacts due to the stopped-flow CD apparatus.

Renaturation at Acidic pH. The rapid and slow phases observed at 222 nm during the refolding of HEL at neutral pH could be interpreted in two ways. They might correspond to a reorganization of the secondary structure resulting in a decrease in the total α-helix content of the protein. Then, because the rate constants of the slow phase at 222, 260, and 289.5 nm are about the same, this reorganization and the final tight packing of the aromatic side chains would occur simultaneously in a cooperative process. Alternatively, the CD changes at 222 nm might result from a contribution of the aromatic side chains to the ellipticity at 222 nm. It would

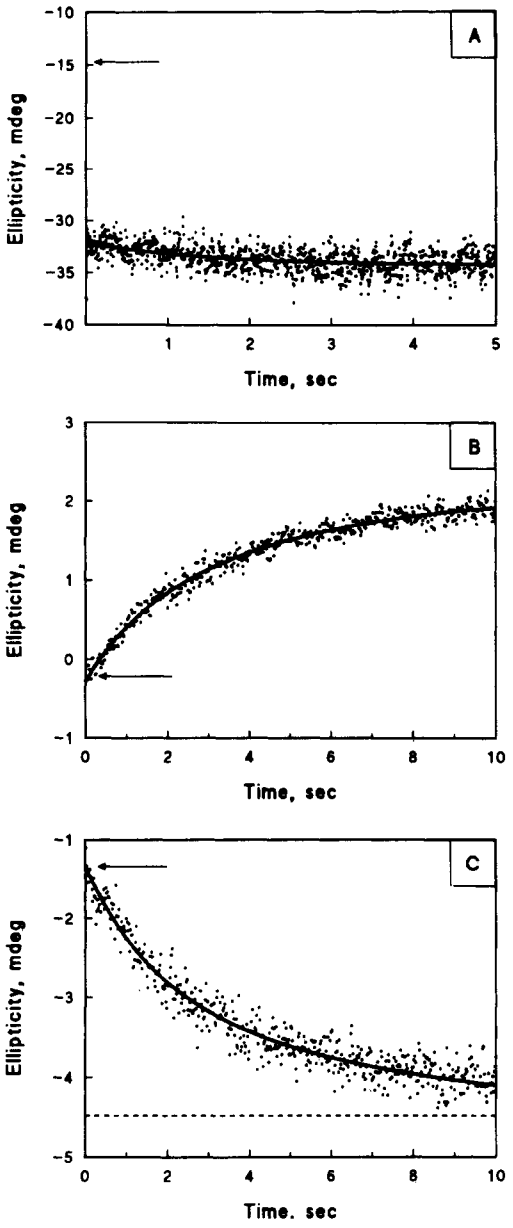

FIGURE 2: Kinetics of ellipticity changes upon folding of HEL at acidic pH. HEL in buffer A containing 6 M GuHCl (from the small syringe) was mixed with buffer A (from the large syringes) in 140 ms. Recording of the ellipticity was triggered at the end of the injection. The fits shown are with biphasic sequential kinetics. The horizontal arrow indicates the ellipticity of unfolded HEL in buffer A (see legend to Figure 1). (A) Ellipticity at 222 nm: 25 μL of denatured HEL (8 mg/mL) and 725 μL of buffer A were injected. The resulting concentration of HEL in the observation cell was 0.27 mg/mL. The sampling interval and filtering constant were 5 ms. The number of kinetics accumulated was 220. (B) Ellipticity at 289.5 nm and (C) ellipticity at 260 nm: 25 μL of denatured HEL (25 mg/mL) and 725 μL of buffer A were injected. The resulting concentration of HEL in the observation cell was 0.8 mg/mL. The sampling interval and filtering constant were 10 ms. The number of kinetics accumulated was 134 at 289.5 nm and 240 at 260 nm.

then reflect only the tight packing of these residues and not a rearrangement of the secondary structure. With the aim of distinguishing these alternatives, we investigated the folding of HEL at acidic pH, hoping that this drastic change in the folding conditions might result in a kinetic uncoupling of the side chain tight packing on the one hand from the formation of secondary structure on the second hand.

HEL, denatured with 6 M GuHCl in buffer A, was diluted 80-fold in buffer A and the CD was monitored at 222 nm to follow the formation of secondary structure. The results of a typical experiment are shown in Figure 2A. As expected,

Table II: Rate Constants and Amplitudes of the Kinetic Phases Observed by CD during the Folding of HEL at Acidic pH[a]

wavelength (nm)	phase	rate constant (s^{-1})	amplitude[b] (%)
222	burst	>250	90
	slow	0.7 ± 0.1	10
260	burst		0
	slow	0.6 ± 0.01	58
	very slow	0.15 ± 0.03	42
289.5	burst		0
	slow	0.9 ± 0.2	43
	very slow	0.23 ± 0.01	57

[a] The kinetic parameters at each wavelength are those obtained for the best fit of the experimental data of Figure 2 to a biphasic process. [b] The amplitudes are expressed as a percentage of the difference between the ellipticities of native and denatured HEL.

the refolding was again reflected by an overall decrease of the ellipticity. The kinetics of the decrease were again complex but showed two major differences with the kinetics at neutral pH. One was that the decrease of the ellipticity was monotonic, without the "overshoot" observed at neutral pH. The second was that the visible part of the kinetics (i.e., after the dead time) was much slower than at neutral pH. Indeed, after a burst phase, representing about 90% of the total CD change that was completed within 6 ms, one could observe a slow decrease which could be satisfactorily fitted to a single exponential. The rate constant of the corresponding phase was about 0.7 ± 0.1 s^{-1}. A similar experiment was performed, monitoring the ellipticity change at 289.5 nm to follow the tight packing of the tryptophan side chains. The kinetics observed are depicted in Figure 2B. The change in the near-UV CD was much slower than the change in far-UV CD. They could be fitted to a two-step sequential model with rate constants of 0.9 ± 0.2 s^{-1} and 0.23 ± 0.01 s^{-1} for the rapid and slow phases, respectively. Finally, monitoring the ellipticity change at 260 nm showed that the environment of the tyrosines and phenylalanines varied according to kinetics that could be fitted to a sequential biphasic model (Figure 2C). The best fit was obtained for amplitudes and rate constants of −1.8 mdeg and 0.6 ± 0.01 s^{-1} for the first phase and −1.3 mdeg and 0.15 ± 0.03 s^{-1} for the second one. These results are summarized in Table II.

Thus, during the refolding of HEL at acidic pH, several phases were observed. Again, a very rapid process occured during the 6-ms dead time of the stopped-flow instrument and resulted in an intermediate with 90% of the native ellipticity at 222 nm and no near-UV ellipticity. This very rapid process was followed by a slow process during which both the far- and near-UV signals changed at similar rates. Performing the renaturation at low pH therefore failed to uncouple the kinetics of far- and near-UV ellipticity regain that follow the initial burst of far-UV CD.

Renaturation at Neutral pH in the Presence of Residual GuHCl. Another possible way of uncoupling the kinetics of formation of secondary and tightly packed tertiary structures was to perform the renaturation of the protein in the presence of varying concentrations of guanidine. Indeed, one could imagine that guanidine would have a differential effect on slowing down these two processes. We therefore investigated the folding of HEL at various GuHCl concentrations and compared the rate constants of the various phases detected at 222 and 289.5 nm. HEL in 6 M GuHCl was diluted 80-fold in buffer N containing GuHCl so that the final GuHCl concentration after mixing ranged between 0.075 and 1.5 M. The overall aspect of the kinetics did not change, but the folding process was indeed slowed down. Figure 3 shows the variation of the rate constants of the "fast" and "slow" phases

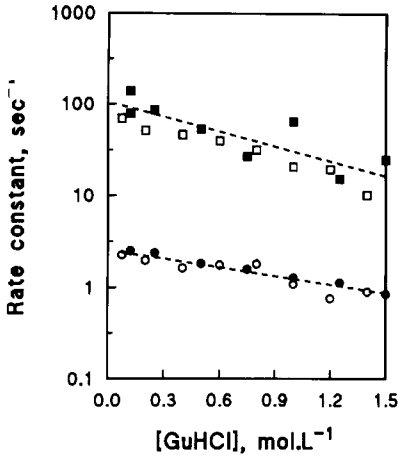

FIGURE 3: GuHCl dependence of the folding rate constants. Experiments similar to those depicted in Figure 1 were repeated in which the buffer contained in the two large syringes was buffer N supplemented with GuHCl. The GuHCl concentration was chosen so that the final residual denaturant concentration after the injection was that indicated in the abscissa. The kinetics were analyzed as indicated in Figure 1, and the resulting rate constants obtained, at each GuHCL concentration, for the rapid and slow phases at 222 nm (open symbols) and 289.5 nm (closed symbols) were plotted as a function of the GuHCl concentration.

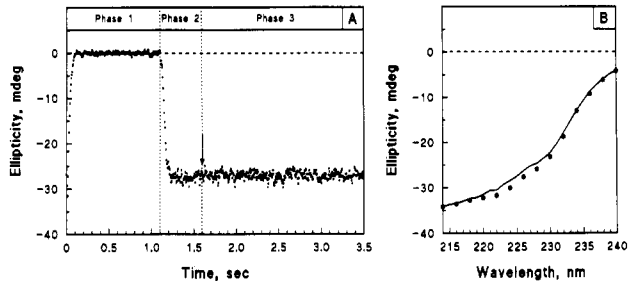

FIGURE 4: Continuous-flow CD spectrum of native HEL. (A) buffer N (400 μL from each large syringe) was injected in 100 ms, and the flow was interrupted during 1 s (phase 1). Then, 50 μL of native HEL (8 mg/mL in buffer N containing 3.5 M GuHCl) from the small syringe and 1.975 mL of buffer N from each large syringe were injected during 500 ms (phase 2), at which time (marked by vertical arrow) the flow was stopped (phase 3). Recording of the ellipticity at 228 nm was triggered before the first injection and continued for 5 s. The sampling interval and filtering constant were 5 ms. The data shown result from the accumulation of 21 kinetics. (B) Experiments identical to that depicted in (A) were repeated at various wavelengths. At each wavelength, the mean ellipticities during phases 1 and 2 were obtained by least-squares fitting to a horizontal line. The difference between the resulting values represents the ellipticity observed for native HEL during the flow and was plotted as a function of the wavelength (●). The solid line represents the spectrum of HEL in the same buffer and at the same concentration, obtained by scanning at equilibrium in the stopped-flow cell. The equilibrium spectrum was obtained as described under Materials and Methods.

observed at the two wavelengths as a function of GuHCl concentration. It can be seen that, at each GuHCl concentration investigated, the rate constants for the slow phases at 222 and 289.5 nm were the same. For the rapid phase, the fit between the data at 222 and 289.5 nm was not as good. But because of the small amplitude of the corresponding signal changes, the differences lie within experimental uncertainties and it appears that GuHCl exerted similar effects on the slow phase detected at both wavelengths. Thus, neither for the rapid phase nor for the slow one was GuHCl found to uncouple the kinetics at 222 and 289.5 nm.

Far-UV CD Spectrum of the Folding Intermediates at 4 ms. From the studies reported above, it clearly appeared that, both at acidic and at neutral pH, the intermediate present at 6 ms shows no near-UV CD. Its aromatic side chains thus appeared to still be in an isotropic environment and were therefore not expected to give any contribution to the far-UV CD spectrum. Having in mind the characterization of the secondary structure of this intermediate, it seemed of interest to obtain its CD spectrum with as much precision as possible. This was done by continuous-flow studies in the following way. HEL was diluted 80-fold by injecting 50 μL of protein solution with 3.95 mL of buffer N over a period of 500 ms. This resulted in a flow rate of 8 mL/s and a dead time of 4 ms. The ellipticity was recorded during and after the injection with a sampling interval and a filtering time constant of 5 ms. The CD signal observed was expected to remain constant throughout the injection period and to represent the ellipticity of the species present 4 ms after the mixing.

It was first checked that ellipticity measurements during the flow could indeed be achieved and did not result in a biased spectrum. For this purpose, the highest GuHCl concentration in which HEL remained native was determined by monitoring the far-UV CD spectrum of HEL at various GuHCL concentrations. It was found that in buffer N, at 20 °C and up to 3.5 M, GuHCl failed to unfold the protein (data not shown). Native HEL in 3.5 M GuHCl was then diluted 80-fold with buffer N according to the continuous-flow protocol outlined above, and the ellipticity was monitored at wavelengths ranging between 214 and 240 nm. Figure 4A shows, that, throughout the injection phase, the ellipticity at 222 nm did not change and also remained constant thereafter. This indicated that the flow by itself did not affect the observed ellipticity. Moreover, the intrinsic ellipticity of HEL at each wavelength was determined by subtracting the ellipticity observed for the buffer (first phase in Figure 4A) from the ellipticity observed for the protein solution during the flow. This resulted in the spectrum marked by symbols in Figure 4B. This spectrum was perfectly consistent with that obtained by conventional scanning of native HEL at equilibrium in the stopped-flow cell. This ascertained that the continuous-flow method could be used to determine the CD spectrum of the species present 4 ms after the mixing.

This method was therefore used to investigate the 4-ms intermediate during the refolding of GuHCl-denatured HEL. Figure 5A shows a typical recording obtained when HEL unfolded in 6 M GuHCl was diluted in buffer N according to the continuous-flow protocol. From such recordings, the intrinsic ellipticity after 4 ms of folding was calculated (see legend to Figure 5) and the far-UV CD spectrum of the 4-ms intermediate was generated (Figure 5B). Its overall aspect markedly differed from that of native HEL (dashed line in Figure 5B). In particular, above 220 nm, the amplitude of the ellipticity of the intermediate was much larger than that of native HEL.

To gain a better understanding of this difference, the evolution of the CD spectrum at later stages of the folding was investigated by analyzing the kinetics of the ellipticity change after interruption of the flow in the "continuous-flow" experiments described above (phase 3 in Figure 5A). It was first verified that the signal evolved toward a final value which was consistent with the ellipticity of the native protein (triangles and dashed line, respectively, in Figure 5B). The kinetics at each wavelength were then analyzed. Each one could be satisfactorily fitted to a biphasic process. Except for a few data points at wavelengths where the amplitude of the change was very small, the rate constant obtained for each phase did not vary significantly throughout the wavelength range investigated (Figure 5C). This suggested that the same kinetic process was reflected by the CD change at all the wavelengths investigated. The average rate constants for the two phases

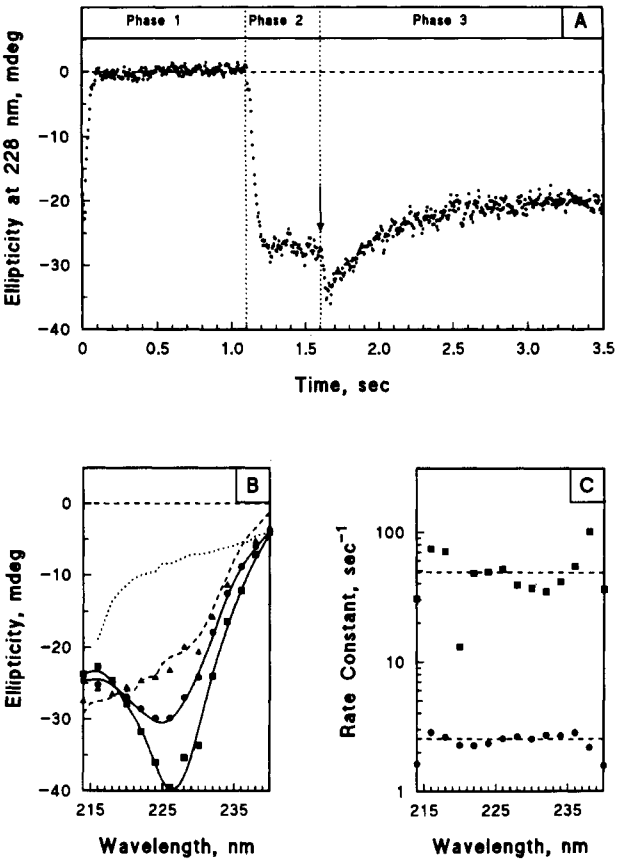

FIGURE 5: Continuous- and stopped-flow CD spectra of HEL folding intermediates. (A) Continuous/stopped-flow kinetics of the CD change at 228 nm. Experiments starting from denatured HEL (8 mg/mL in 6 M GuHCl) were achieved, using a protocol identical to that described in Figure 4A. The kinetics depicted resulted from 21 accumulations. (B) Far-UV CD spectra of unfolded, 4-ms refolded, and completely refolded HEL. From the continuous-flow part of experiments similar to that shown in (A), the ellipticity during the flow (i.e., of the intermediates present at 4 ms of folding) was obtained as described in Figure 4 and was plotted as a function of the wavelength (●). The final ellipticity observed at the plateau (i.e., at the end of the folding process) was also plotted as a function of the wavelength (▲). Finally, at each wavelength, the amplitude of the ellipticity change during the rapid phase was obtained from a constrained fitting using the average rate constants determined over the wavelength range investigated (see panel C) and the ellipticity at 4 ms determined from the continuous-flow measurements. The result was plotted as a function of the wavelength (■). The spectra of unfolded (···) and native (- - -) HEL recorded at equilibrium (see Materials and Methods) are also shown. (C) Wavelength dependence of the observed folding rate constants. The data obtained at each wavelength from experiments similar to that shown in (A) were used to determine the best fit with triphasic kinetics in which the first phase corresponds to the burst. The rate constants of the rapid and slow phases were plotted as a function of the wavelength. The horizontal dashed lines show the average value, over the wavelength range investigated, of these rate constants (i.e., 44 ± 6 s^{-1} for the rapid phase and 2.8 ± 0.1 s^{-1} for the slow phase). The points which significantly deviate from the dashed line correspond to wavelengths at which the total ellipticity change observed during the folding is very small, and hence the fitting is hardly precise.

were therefore determined (dashed lines in Figure 5C), and for each wavelengths, these rate constant as well as the ellipticity at 4 ms determined from the continuous-flow measurements were introduced in a constrained, two-exponential fitting of the ellipticity amplitude as a function of time. From the fittings obtained, one could extract the intrinsic ellipticity of the intermediate formed at the end of the rapid phase. The CD spectrum thus obtained is represented by the squares in Figure 5B.

Similarly, back extrapolation of the fitted curves to –4 ms (i.e., to the time zero of folding) yielded the amplitude of the

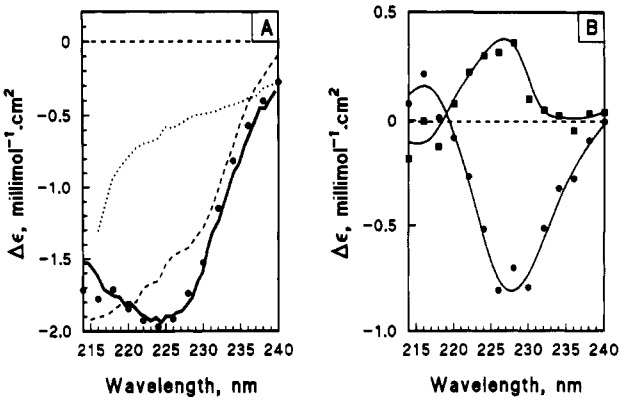

FIGURE 6: Far-UV CD spectra of the 4-ms intermediate and of the S–S bonds. (A) "Initial" CD spectrum of the burst intermediate. At each wavelength investigated, the rapid phase of the constrained fit described in Figure 5B was extrapolated to –4 ms (i.e., to the time when folding was initiated in the mixer of the stopped-flow apparatus). The resulting ellipticity, which corresponds to the ellipticity at the end of the burst phase resolved from the contributions of the rapid and slow phases, was converted to Δε/residue and plotted as a function of the wavelength (●). The solid line (—) represents the pure peptide bond contribution to the far-UV CD spectrum of native HEL, calculated by linear combination of the four reference spectra for α-helix, β-structure, turns, and coil determined by Brahms and Brahms (1980) using the secondary structure assignment for HEL of Kabsch and Sander (1983). The CD spectra of unfolded (···) and native (- - -) HEL are shown for comparison. (B) Contribution of S–S bonds to the far-UV CD spectrum of folding intermediate and native HEL. The ellipticity change associated with the rapid phase was estimated from the constrained fit described in Figure 5B and was converted to Δε/residue and plotted as a function of the wavelength (●). The resulting spectrum corresponds to the difference spectrum between the end of the fast phase and the initial spectrum shown in (A). Similarly, the difference between the CD spectrum of native HEL and the initial CD spectrum, obtained from the algebraic sum of the amplitudes of the rapid and slow phases, was plotted as a function of the wavelength (■).

burst phase cleared from the contribution of the rapid phase. The corresponding spectrum, shown in Figure 6A, will from now on be referred to as the "initial" intermediate spectrum. When this spectrum was subtracted from that of the intermediate resulting from the rapid phase, one obtained the difference spectrum shown in Figure 6B. It corresponds to the CD change that accompanies the folding step involved in the rapid phase and that is responsible for the overshoot observed in the kinetics. By comparison with the results of Kosen et al. (1981), this spectrum suggests that disulfide bonds may be responsible for the CD change in the far-UV during the rapid phase, though a contribution from aromatic side chains may not be excluded (see the Discussion section).

DISCUSSION

The results described in this report demonstrate that coupled continuous-flow and stopped-flow CD measurements provide reliable CD spectra of intermediates in a wide time range, extending from as early as 4 ms up to the end of the folding process. Investigating the rates of formation and the spectral characteristics of the species obtained at different stages of the folding therefore becomes possible and should provide a better understanding of the folding process.

A detailed analysis of the time course of the ellipticity change was achieved at three wavelengths, 222, 260, and 289.5 nm, usually considered as characteristic, respectively, of the peptide bonds, the tyrosine or phenylalanine side chains, and the tryptophan side chains. This analysis led us to distinguish three folding phases: the "burst" phase ($k > 250\ s^{-1}$), resulting in the "initial" CD spectrum in the far-UV and no CD in the near-UV; the "rapid" phase (k = 25–80 s^{-1}), associated with

an overshoot in the amplitude of the ellipticity at 222 nm and with the appearance of ellipticity in the near-UV; and the "slow" phase (k = 2.5 s^{-1}) that involves changes in both the far- and near-UV regions and leads to the nativelike CD spectrum. The rate constants and relative amplitudes associated with these phases at each wavelength are summarized in Table I.

A major problem in interpreting such results is to relate a CD change observed at a given wavelength with a specific type of conformational rearrangement. Thus, in the present study of lysozyme folding, the ellipticity at 222 nm undergoes detectable changes during the three phases described above. Do these CD changes reflect secondary structure modifications associated with the three phases, which is the usual interpretation? Or do they also reflect the tight packing of side chains that might occur without rearrangement of the secondary structure? As shown above, attempts to uncouple the far- from the near-UV CD signals during the rapid and slow phases were unsuccessful. Neither a severe pH change nor slowing down to varying extents the folding kinetics by the presence of variable amounts of GuHCl resulted in a differential effect on the kinetics observed in the far- and near-UV. This could be interpreted as an indication that the folding steps involved in these two phases are highly cooperative transitions involving tightly coupled secondary and tertiary structure rearrangements. Alternatively, however, the rapid and slow phases detected in the far-UV could be independent of secondary structure changes and might result essentially from a contribution of the side chains to the far-UV CD signal.

This alternative could be solved by an analysis of the wavelength dependence of the far-UV ellipticity changes associated with each phase. Indeed, from the experimental data we obtained, three far-UV CD spectra can be obtained: that of the species formed during the burst phase and characterized by the "initial" spectrum depicted in Figure 6A, that associated with the structural transition occurring during the rapid phase and characterized by the difference spectrum shown in Figure 6B, and finally, that of the native protein obtained at the end of the folding process (see Figure 5B).

The "initial" spectrum (Figure 6A) has been obtained by back extrapolation of the CD kinetics to time zero. This removes from the experimental spectrum at 4 ms any ellipticity contribution from molecules that have undergone the rapid transition within the first 4 ms. Deconvolution of the kinetics of the ellipticity changes at 260 and 289.5 nm yields initial values which, within the experimental uncertainties, coincide with the ellipticity of the denatured protein. This indicates that, at the end of the burst phase, essentially all the cystinyl and aromatic side chains (the only chromophores likely to contribute to the near-UV ellipticity in proteins) are still in a symmetrical environment. The contribution of disulfides and aromatic side chains to the CD is about 1 order of magnitude higher in the far-UV than in the near-UV (Takagi & Ito, 1972; Adler et al., 1973). However, in our experiments, the CD changes were investigated at protein concentrations 5-fold higher for the near-UV (0.5 mg/mL) than for the far-UV studies (0.1 mg/mL). Thus, in our experiments, total ellipticity changes of comparable amplutides were expected to be observed in the two wavelength regions. That no detectable ellipticity could be observed at 0.5 mg/mL in the near-UV at the end of the burst phase therefore renders it unlikely that the aromatic side chains might bring an important contribution to the CD signal observed at 0.1 mg/mL in the far-UV. Moreover, disulfide bonds generate an important CD signal in the 215–240-nm region only when their dihedral angle is close to 90° and the wavelength of the maximum and the sign and the amplitude of the CD signal are very sensitive to deviations of this angle around this value (Rauk, 1984). It seems quite unlikely that the disulfide dihedral angles would already be constrained to near 90° at a stage of the folding where close packing is clearly absent, and therefore that the disulfide chromophore would bring an important contribution to the far-UV initial CD spectrum. As for the aromatic side chains of the three tyrosines and six tryptophans of HEL, they may also contribute to the initial spectrum in the 220–230-nm wavelength range. However, studies on model compounds have shown that the $\Delta\epsilon$ of the aromatic side chains in this wavelength range is only about 3 per aromatic residue (Adler et al., 1973) which, even in the unlikely situation where the ellipticities of all the aromatic residues would be cumulative, would result in a $\Delta\epsilon$ of about 27 per HEL molecule. Thus a maximum of 11% only of the total ellipticity ($\Delta\epsilon$ = −245 per molecule at 220 nm) observed at the end of the burst phase of HEL refolding could eventually be accounted for by a contribution from the aromatic side chains. It therefore appears reasonable to conclude that the major contribution to the far-UV CD initial spectrum comes from the peptide bonds and that this spectrum reflects essentially the conformational state of the polypeptide backbone in the molecular species formed within the first 4 ms of the folding process. The initial spectrum has been compared with that predicted for the contribution of the peptide bond to the far-UV CD in native lysozyme. These two spectra are in excellent quantitative agreement (see Figure 6A), which strongly suggests that the nativelike peptide bond ellipticity is already essentially present after only 4 ms of refolding. This conclusion is strongly supported by the following observation. The difference CD spectra associated with the rapid and slow phases of HEL folding both exhibit an intense but relatively narrow band centered at 227–228 nm. On the contrary, after the burst phase, there are only small changes of the ellipticity in the 215–222-nm region, which, in the wavelength range investigated here, is by far the most sensitive to changes in the protein secondary structure. This confirms that, after the burst phase, the peptide bond contribution to the far-UV CD does not change significantly. Thus, the intermediate species that is formed in less than 4 ms appears to already exhibit an essentially nativelike overall content in α-helices, β-structures, and turns.

Let us now discuss the difference spectrum, with a major negative peak centered at 227–228 nm and a minor positive peak centered at about 215 nm (Figure 6B), that is associated with the rapid phase. This phase is clearly related to changes in the conformation and/or environment of side chains, as reflected by the evolution of the ellipticities in the near-UV at 260 and 289.5 nm (see Table I). The only side chains likely to also contribute to the ellipticity in the 225–230-nm region are the tyrosyl and tryptophanyl side chains and the disulfide bonds. The similarity of the positions and relative amplitudes of the two extrema of the difference spectrum in Figure 6B with those reported for the difference spectrum between native BPTI and BPTI in which cysteines 14 and 38 have been either reduced or carboxymethylated [Figure 4 in Kosen et al. (1981)] already suggests that disulfides may be the chromophores responsible for the far-UV CD change during the rapid phase. Moreover, the total ellipticity change during this phase corresponds to a $\Delta\epsilon$ of about −100 per HEL molecule. This large differential absorbance change is not likely to be caused by the tyrosyl and tryptophanyl side chains since, as pointed out above, the maximum contribution expected from these side chains does not exceed a $\Delta\epsilon$ of 27 per HEL molecule. On

the contrary, it seems compatible with a contribution from disulfides since the $\Delta\epsilon$ associated with the reduction of a single disulfide bond in BPTI is about 20 per molecule (Kosen et al., 1981) and since HEL contains a total of four disulfide bonds. Such major contributions of the disulfide chromophore to the CD band in the 225–230-nm region have already been well documented in the case of the elapid toxins (Hider et al., 1988). It would therefore be tempting to conclude that the major contribution to the ellipticity change observed around 227–228 nm during the fast folding phase of HEL comes from disulfide bonds. The CD band that appears during the rapid phase of HEL folding is negative, while that reported for the disulfide chromophore in BPTI or the elapid toxins is positive (Kosen et al., 1981; Hider et al., 1988). However, the sign of the CD signal of disulfide bonds in the 185–400-nm spectral region was shown to be directly related to the sign and the value of the CSSC dihedral angle ϕ. For instance, the negative band in the 227–228-nm region could be attributed to four CSSC motifs with a dihedral angle close to 90° in the P (right-handed helix) chiral conformation (Neubert & Carmack, 1974). Moreover, strong negative CD bands in the 225–230-nm region have been observed in a variety of disulfide cyclic peptides of various lengths containing a proline residue (Venkatachalapathi et al., 1982; Ravi & Balaram, 1983, 1984; Kishore et al., 1988) and HEL contains two such proline-containing disulfide loops (residues 64–80 and 76–94). Thus, disulfide bonds indeed are likely to be responsible for a major part of the far-UV CD change observed during the rapid phase.

Finally, the difference spectrum between native HEL and the species formed within the first 4 ms of folding much resembles in shape, wavelength of the maximum differential absorbance, and sign of the signal those clearly attributed by Kosen et al. (1981) or by Hider et al. (1988) to disulfide bonds. The amplitude of the signal is about twice that reported by Kosen et al. (1981) for the contribution of a single disulfide bond in native BPTI. From the work of Rauk (1984) and of Neubert and Carmack (1974), it appears that the amplitudes, signs, and wavelength of the maximum for the near- and far-UV CD bands of disulfides vary considerably with the dihedral angle in the CSSC motif. In native HEL, two disulfides have the M chirality and large ϕ angles (123° and 153°, respectively, for the 6–127 and the 30–115 disulfides), while the two others have the P chirality and smaller ϕ angles (101° and 112°, respectively, for the 64–80 and the 76–94 disulfides). Thus, all the disulfide bonds in native HEL are constrained away from their 90° stable conformation in very different ways. Therefore, the sign and intensity of the CD in the 225–230-nm region cannot be readily predicted and compared with those of the CD bands in other disulfide-containing proteins. Thus, in spite of the fact that HEL has two M and two P disulfides, it still seems quite plausible that a major part of the CD band centered at 227–228 nm in native HEL may be due to the disulfide chromophore.

Consequently, though again this should be considered only as an approximation since aromatic side chains are also likely to slightly contribute to the far-UV ellipticity, we shall conclude that the burst, rapid, and slow phases observed by monitoring the far-UV CD during the refolding of HEL correspond respectively to the appearance of a "pure" peptide bond spectrum, to the appearance of disulfide bond(s) constrained in a nonnativelike conformation that gives rise to the intense negative abnormal differential absorbance at 227–228 nm, and finally to an isomerization of the disulfide bonds toward a conformation with the dihedral angle and the chirality found in the native protein.

The molecular species formed within the first 4 ms of the folding process have an approximately nativelike content in secondary structure (as evidenced from the initial spectrum), no tight packing of the side chains (as evidenced by the near-UV CD for the cystines and the aromatic residues) and are likely to be maintained in a condensed state by their four native disulfide bonds. Such properties are characteristic of a folding intermediate, the "molten globule" (Ptitsyn, 1973; Ohgushi & Wada, 1983), which is thought to be a general intermediate in the folding of proteins (Kuwajima, 1989; Ptitsyn et al., 1990). The next step in the folding of HEL (the rapid phase) is associated with a large ellipticity change at 227–228 nm that is likely to arise mainly from a constraint on some of the four S–S bonds of the molecule. This transient constraint on S–S bonds (and perhaps also some transient exposure of aromatic side chains to a nonnative asymmetrical environment), rather than a rearrangement of the secondary structure, is clearly responsible for the transient overshoot observed in the kinetics of far-UV CD changes. The last step in the folding of HEL (the slow phase) clearly corresponds to the tight packing of the aromatic side chains and to the relaxation of the nonnativelike constraints on the S–S bonds.

Why should the very rapidly formed molten globule, with an apparently nativelike secondary structure, go through a conformation with nonnative constraints on its disulfide bonds before the final tight packing of the polypeptide chain can take place? As discussed above, the strong negative CD band observed in this intermediate conformation may have the same origin as that observed in cyclic disulfide peptides that contain the Pro-X or X-Pro sequence and that has been attributed to a type I or II β-turn stabilized in these peptides by the disulfide bond (Kishore et al., 1988). The two short disulfide loops of HEL may perhaps adopt this conformation during the rapid phase and give rise to the negative CD band at 227–228 nm. At this stage, the S–S bonds would restrict considerably the relative movements of the secondary structure elements they connect within the molten globule. Then, the disulfide bonds would have to be distorted to permit a transient swelling of the structure, and thereafter, the correct docking and tight packing of the corresponding secondary structure elements. Alternatively, one could imagine that, though the molten globule formed in less than 4 ms has a nativelike overall secondary structure content, the location of the secondary structure elements along the sequence would be different from that of the native conformation. The transition from a wrong to the right pattern of secondary structure elements would then require a distortion of the disulfide bonds. Though the first model seems by far more plausible, and in line with the current observation (Udgaonkar & Baldwin, 1988; Roder et al., 1988, Bycroft et al., 1990; Briggs & Roder, 1992) that only nativelike secondary structure patterns can be detected by pulsed amide proton protection in folding intermediates, one cannot entirely rule out the latter model. Indeed, CD stopped-flow studies have detected secondary structure elements that are formed earlier than those observed by NMR after pulsed proton labeling experiments (Elöve et al., 1992). Yet, it would be a highly unlikely coincidence if the secondary structure content of the 4-ms intermediate were nativelike and the secondary structure pattern were grossly nonnative. It should be pointed out that, in the two models proposed above, disulfide isomerization seems to be involved in the later steps of HEL folding. This suggests that disulfide bonds might be responsible for the slow refolding kinetic phase observed for human lysozyme (a protein closely related to HEL), for which Herning et al. (1991) showed that it does not result from proline cis–trans isomerization.

The main conclusions that one can draw from the work reported here are the following: (1) The combined use of continuous-flow and stopped-flow CD techniques has permitted us to resolve the contribution of the peptide backbone (secondary structure) from that of the side chains (cystines and aromatic residues) to the far-UV ellipticity during the folding of HEL. (2) The overshoot of ellipticity at 222 nm that follows the burst phase during the refolding of HEL is not due to a rearrangement of the secondary structure but probably to a transient constraint on disulfide bonds. A similar effect of disulfide bonds might also explain the previously reported overshoot in far-UV CD during the folding of β-lactoglobulin (Kuwajima et al., 1987). A detailed spectral study should therefore be performed before one can interpret in a reliable way the ellipticity changes observed during protein folding. (3) During the refolding of GuHCl-unfolded HEL with its native disulfides intact, the nativelike secondary structure pattern is formed in less than 4 ms.

The latter conclusion is, at present, only tentative (see above). If it were confirmed, it would raise the question of why the native secondary structure of HEL is formed so much faster than for other proteins that have been investigated (Udgaonkar & Baldwin, 1988; Roder et al., 1988, Bycroft et al., 1990; Briggs & Roder, 1992). Several answers can be brought to this question. The present study has been performed at 20 °C, neutral pH, and in the absence of significant amounts of residual denaturing agent. On the contrary, the studies by pulsed proton labeling coupled to NMR (see references just quoted) were performed at more acidic pH, low temperature, and usually in the presence of significant concentration of denaturant, conditions that are known to slow down the folding process. Also, it should be noted that, like for bovine ribonuclease (Udgaonkar & Baldwin, 1988), the present studies were performed with nonreduced HEL. The presence of four native disulfide bonds may also contribute to speeding up the formation of the nativelike secondary structure. In this respect, and since reduced HEL can be refolded and oxidized with relatively high efficiency (Epstein & Goldberger, 1963; Yutani et al., 1968; Saxena & Wetlaufer, 1970; Goldberg et al., 1991), it will be of interest to investigate its folding by the approach described here. This should allow one to assess the role of the disufide bonds during the early steps of the folding process. But the most likely interpretation is that, as already reported for cytochrome *c* (Elöve et al., 1992), the very early secondary structure elements detected by CD stopped-flow during the folding of HEL may be formed much faster than even the first stable hydrogen-bonded structures detected by pulsed proton labeling. Recent results by Radford et al. (1992) lend support to this conclusion.

REFERENCES

Adler, Greenfield, & Fassman (1973) *Methods Enzymol. 27*, 729.

Aune, K. C., & Tanford, C. (1969) *Biochemistry 8*, 4586–4590.

Baldwin, R. L. (1991) in *Protein Conformation*, Ciba Foundation Symposium 161, pp 190–205, Wiley, Chichester, England.

Baldwin, R. L., & Roder, H. (1991) *Curr. Biol. 1*, 218–220.

Blake, C. C. F., Koenig, D. F., Mair, G. A., North, A. C. T., Phillips, D. C. & Sarma, V. R. (1965) *Nature (London) 206*, 757–759.

Brahms, S., & Brahms, J. (1980) *J. Mol. Biol. 138*, 149–178.

Briggs, M. S., & Roder, H. (1992) *Proc. Natl. Acad. Sci. U.S.A. 89*, 2017–2021.

Bycroft, M., Matouschek, A., Kellis, J. T., Jr., Serrano, L., & Fersht, A. (1990) *Nature 346*, 488–490.

Chaffotte, A. F., Cadieux, C., Guillou, Y., & Goldberg, M. E. (1992) *Biochemistry 32*, 4303–4308.

Creighton, T. E. (1990) *Biochem. J. 270*, 1–16.

Dill, K. A.(1985) *Biochemistry 24*, 1501–1509.

Dobson, C. M., & Evans, P. A. (1984) *Biochemistry 23*, 4267–4270.

Elöve, G. A., Chaffotte, A. F., Roder, H., & Goldberg, M. E. (1992) *Biochemistry 31*, 6876–6883.

Epstein, J. C., & Goldberger, R. F. (1963) *J. Biol. Chem. 238*, 1380–1383.

Goldberg, M. E., Rudolph, R., & Jaenicke, R. (1991) *Biochemistry 30*, 2790–2797.

Herning, T., Yutani, K., Taniyama, Y., & Kikuchi, M. (1991) *Biochemistry 30*, 9882–9891.

Hider, R. C., Drake, A. F., & Tamiya, N. (1988) *Biopolymers 27*, 113–122.

Ikeguchi, M., Kuwajima, K., Mitani, M., & Sugai, S. (1986) *Biochemistry 25*, 6965–6972.

Kabsch, W., & Sander, C. (1983) *Biopolymers 22*, 2577–2637.

Kato, S., Okamura, M., Shimamoto, N., & Utiyama, H. (1981) *Biochemistry 20*, 1080–1085.

Kim, P. S., & Baldwin, R. L. (1982) *Annu. Rev. Biochem. 51*, 459–489.

Kim, P. S., & Baldwin, R. L. (1990) *Annu. Rev. Biochem. 59*, 631–660.

Kishore, R., Raghothama, S., & Balaram, P. (1988) *Biochemistry 27*, 2462–2471.

Kosen, P. A., Creighton, T. E., & Blout, E. R. (1981) *Biochemistry 20*, 5744–5760.

Kuwajima, K. (1989) *Proteins: Struct., Funct., Genet. 6*, 87–103.

Kuwajima, K., Hiraoka, Y., Ikeguchi, M., & Sugai, S. (1985) *Biochemistry 24*, 874–881.

Kuwajima, K., Yamaya, H., Miwa, S., Sugai, S., & Nagamura, T. (1987) *FEBS Lett. 221*, 115–118.

Kuwajima, K., Garvey, E. P., Finn, B. E., Matthews, C. B., & Sugai, S. (1991) *Biochemistry 30*, 7693–7703.

Labhardt, A. M. (1986) *Methods Enzymol. 131*, 126–135.

Manning, M. C., & Woody, R. W. (1989) *Biochemistry 28*, 8609–8613.

Neubert, L. A., & Carmack, M. (1974) *J. Am. Chem. Soc. 96*, 943–945.

Pflumm, M., Luchins, J., & Beychok, S. (1986) *Methods Enzymol. 130*, 519–534.

Oas, T. G., & Kim, P. S. (1988) *Nature 336*, 42–48.

Ohgushi, M., & Wada, A. (1983) *FEBS Lett. 164*, 21–24.

Ptitsyn, O. B. (1973) *Vestn. Akad. Nauk. SSSR 5*, 57–68.

Ptitsyn, O. B., Pain, R. H., Semisotnov, G. V., Zerovnik, E., & Razgulyaev, O. I. (1990) *FEBS Lett. 262*, 20–24.

Radford, S. E., Dobson, C. M., & Evans, P. A. (1992) *Nature* (in press).

Rauk, A. (1984) *J. Am. Chem. Soc. 106*, 6517–6524.

Ravi, A., & Balaram, P. (1983) *Biochim. Biophys. Acta 745*, 301–309.

Ravi, A., & Balaram, P. (1984) *Tetrahedron 40*, 2577–2583.

Redfield, C., & Dobson, C. M. (1988) *Biochemistry 27*, 122–136.

Roder, H., Elöve, G. A., & Englander, S. W. (1988) *Nature 335*, 700–704.

Saxena, V. P., & Wetlaufer, D. B. (1970) *Biochemistry 9*, 5015–5023.

Sears, D. W., & Beychok, S. (1979) in *Physical Principles and Techniques of Protein Chemistry* (Leach, S. J., Ed.) Part C, pp 445–593, Academic Press, New York.

Takagi, T., & Ito, N. (1972) *Biochim. Biophys. Acta 257*, 1–10.

Tanford, C. (1970) *Adv. Protein Chem. 24*, 1–95.

Tanford, C., Pain, R. H., & Otchin, N. S. (1966) *J. Mol. Biol. 15*, 489–504.

Udgaonkar, J. B., & Baldwin, R. L. (1988) *Nature 335*, 694–699.

Venkatachalapathi, Y. V., Prasad, B. V. V., & Balaram, P. (1982) *Biochemistry 21*, 5502–5509.

Yutani, K., Yutani, A., Imanishi, A., & Isemura, T. (1968) *J. Biochem. (Tokyo) 64*, 449–453.

Registry No. Lysozyme, 9001-63-2.